Environmental Fluid Mechanics **1:** 49–69, 2001.

Large-Eddy Simulations of the Atmospheric Boundary Layer Using a New Subgrid-Scale Model

II. *Weakly and moderately stable cases*

FENG DING, S. PAL ARYA and YUH-LANG LIN
Department of marine, Earth and Atmospheric Sciences, North Carolina State University, Raleigh, NC 27695-8208, U.S.A.

Received 14 August 2000; accepted in revised form 5 October 2000

Abstract. A series of simulations under weakly to moderately stable boundary layers (SBLs) have been performed using the proposed subgrid-scale (SGS) model implemented into the Terminal Area Simulation System (TASS). The proposed SGS model incorporates some aspects of the two-part eddy viscosity SGS model of Sullivan *et al.* (1994) and further refinements which include the dependence of SGS mixing length on stratification, two-part separation of the SGS eddy diffusivity of heat, and more realistic empirical forms of Monin–Obukhov similarity functions. The potential temperature profiles from simulations clearly show a three-layer structure: a stable surface layer of strong gradients, a middle layer of small gradients, and an inversion layer on the top. The wind speed profiles show the formation of low level jet (LLJ). However, the sub-layer structures under moderately SBLs differ from those under weakly SBLs. Both the momentum and heat fluxes decrease almost linearly in the lower part of the SBL. The near surface values of the normalized turbulent kinetic energy (TKE/u_*^2) in all simulations are about 4 which is much less than the typical value of 5.5 under the neutral condition. The decay of turbulence first occurs in the area with large values of Richardson number ($R_i > 0.2$). Generally, instantaneous values of the TKE and R_i at the various grid points are negatively correlated, but there is not a unique relationship between the two parameters.

1. Introduction

Although the large-eddy simulation (LES) approach has been extensively and successfully used for modeling boundary flows under neutral, unstable and convective conditions for more than twenty years, its application to simulate stable boundary layer (SBL) only started recently when super computer's CPU speed and memory size allowed small enough grid size in the model.

Mason and Derbyshire (1990) presented a series of simulations of the SBL over a uniform, flat terrain. The model adopted in their studies was the same as that described by Mason (1989) in his LES study of the CBL. Their subgrid-scale (SGS) model was a modified Smagorinsky model where the eddy-viscosity was related to flux Richardson number. The critical flux Richardson number was specified as 0.33, above which the subgrid eddy viscosity vanished. The subgrid Prandtl number was also specified a constant value of 0.5 in their model. They used a horizontal grid resolution of 12 m and vertical grid size varying from 0.6 m at the surface to 17 m at 320 m and 26 m above 640 m. The simulation time was 2 hours after the initial neutral boundary layer was subjected to a constant cooling rate or surface

heat flux. The simulated structure was found to be consistent with Nieuwstadt's (1984) local scaling hypothesis and the results of Brost and Wyngaard's (1978) second-order closure model.

Brown *et al.* (1994) extended Mason and Derbyshire's (1990) work to a wider range of stabilities (up to Richardson number $R_i = 0.5$). They used a revised version of the stochastic backscatter SGS model which was proposed by Mason and Thomson (1992). The simulations without backscatter were also conducted for comparisons. The simulated values of the Obukhov length ($L > 31$ m) indicate that only mild to moderate stability conditions were represented in their simulations of the SBL. The use of stochastic backscatter in the SGS model resulted in better resolution of turbulence and more realistic velocity and temperature profiles in the surface layer, which were consistent with the empirical Monin–Obukhov similarity profiles. However, their results appeared to be quite sensitive to the subgrid parameterization and also somewhat sensitive to domain size. The use of stochastic backscatter also increased computing cost.

Kaltenbach *et al.* (1994) simulated the homogeneous turbulence in neutral and stably stratified flows using LES. They used a simple Smagorinsky SGS model. The gradient Richardson number was varied from 0 to 1. They also performed direct numerical simulations (DNS) with $R_i = 0.13$, 0.25, and 0.5. For $R_i = 0.13$ (smaller subcritical value), LES and DNS results agreed well, but diverged for the supercritical Richardson number.

SGS model is a critical component for any successful LES, especially for the simulation of SBL. Its importance is further demonstrated by Andren (1995), who simulated weakly stratified boundary layers, one with a neutral layer aloft and the other capped by an inversion. Andren compared the LES results for the latter for two different SGS models, the one based on the turbulent kinetic energy (TKE) model (Moeng, 1984) and the other two-part eddy-viscosity model proposed by Sullivan *et al.* (1994). He used a domain of 600 m $\times$ 400 m $\times$ 500 m with a grid of 96 $\times$ 96 $\times$ 96 points. The simulations were run over a relatively short period of two hours of which the last hour was used to calculate mean fields and turbulence statistics. It is shown that the mean gradients near the surface are better simulated with the refined SGS model and the two-part eddy-viscosity model proposed by Sullivan *et al.* (1994) is comparable in accuracy to the bascatter model of Brown *et al.* (1994). The turbulent fluxes and variances and their budgets have also been successfully simulated by Andren (1995) using the SGS model of Sullivan *et al.* (1994).

Recently, Kosovic (1997) developed a nonlinear SGS model and tested it with some simulations. He also compared the results among several SGS models. He showed that non-dimensional wind speed and temperature gradients obtained using his nonlinear SGS model followed their empirical similarity forms more closely. But, since more terms are involved in the nonlinear model than in a linear model, Kosovic's model requires more computational resources. Using this nonlinear model, Kosovic and Curry (2000) performed a series of simulations of SBL us-

ing the Beaufort Sea Arctic Stratus Experiment (BASE) dataset to impose initial and boundary conditions. They analyzed the evolution of the mean wind, potential temperature and turbulence profiles as well as the TKE budget. Good agreement was found between the LES results and the observations. They also studied the dependence of the stable boundary layer height on the various flow parameters.

In this study, the LES version of Terminal Area Simulation System (TASS-LES) model with a proposed new SGS model, is used for the simulation of SBL. The proposed SGS model is based on Sullivan *et al.*'s (1994) two-part eddy viscosity concept, but without their TKE closure approach; instead, the simpler first-order closure approach is used. The same expression for mean-field eddy viscosity at the first grid level (z_1) is used. However, a different expression based on the SGS momentum flux profile is derived for the grid levels above z_1 (see Ding *et al.*, 2000). To simulate the SBL, however, further refinements are made in the expressions of mixing length, and the diffusivity for heat is also separated into a fluctuating part (ν_θ) and mean-field part (ν_Θ). A series of simulations are performed under the weak to moderate stability conditions. The results are analyzed and compared with results from other investigators.

2. Proposed SGS Model in TASS

The Terminal Area Simulation System (TASS) was originally developed by Proctor (1987) for the study of thunderstorms and microbursts (Proctor, 1988). After some modifications, it became a LES model for the simulation of the atmospheric boundary layer (ABL) (Schowalter *et al.*, 1996). Originally, a modified Smagorinsky first-order closure was used in LES version of TASS model. While it successfully simulated buoyancy-dominated unstable and convective boundary layers, simulations for shear-dominated and neutral boundary layers were deemed somewhat inferior (Ding *et al.*, 2000).

2.1. TWO-PART EDDY VISCOSITY MODEL

In order to simulate the shear-dominated, neutral and stable boundary layers, a new SGS model based on the two-part eddy viscosity SGS model of Sullivan *et al.* (1994) has been developed and implemented into TASS-LES model. In this proposed SGS model, the eddy-viscosity is separated into a fluctuating part (ν_t) and a mean-field part (ν_T), and the equations for computing mean-field eddy viscosity are based on the surface layer similarity theory. For the sake of simplicity, the TKE equation is not included and the model still uses the first-order closure. The proposed SGS model uses the same expression for estimating mean-field eddy viscosity at the first grid level z_1 above the surface as derived by Sullivan *et al.* (1994), however, a different expression based on the SGS momentum flux profile is used above z_1. Details are given in the companion paper by Ding *et al.* (2000) together with simulation results for slightly unstable and neutral ABLs.

2.2. REFINEMENT OF MIXING LENGTH PARAMETERIZATION

Under stable conditions, the mixing length is significantly reduced and so is the SGS turbulent kinetic energy. The expression suggested by Deardorrff (1980) is used here:

$$l = \frac{0.76e^{1/2}}{\left(\frac{g}{\Theta_0}\frac{\partial\Theta}{\partial z}\right)^{1/2}}. \tag{1}$$

Equation (1) is used in both the SBL and the elevated inversion layer above the so-called residual layer. Here, Θ_0 is a reference potential temperature which is taken as the mean potential temperature. The SGS turbulent kinetic energy e is estimated from the SGS eddy viscosity model.

Following Deardorff (1970), e can be expressed as a function of mixing length and eddy viscosity as:

$$e = \frac{(1/3)\,\nu_t^2}{((c_1/c_s)\,l)^2}, \tag{2}$$

where $c_1 = 0.094$, and c_s is the Smagorinsky constant.

Combining Equation (2) with the expression for the fluctuating SGS eddy viscosity (Ding *et al.*, 2000),

$$\nu_t = l^2\left[\left(2S_{ij}S_{ij}\right)\left(1 - R_f\right)\right]^{1/2}, \tag{3}$$

one obtains

$$e = \frac{1}{3}\left(\frac{c_s}{c_1}\right)^2 \nu_t\sqrt{2S_{ij}S_{ij}\left(1 - R_f\right)}. \tag{4}$$

Thus, in the proposed SGS model, e is calculated from the values of S_{ij}, R_f and ν_t at the previous time step.

2.3. TWO-PART EDDY DIFFUSIVITY MODEL

We also use a two-part eddy diffusivity of heat to parameterize the SGS vertical heat flux. The approach adopted here is similar to that of Saiki *et al.* (1999). The expression of the SGS vertical heat flux is separated into two parts:

$$\overline{w\theta} = -\gamma\,\nu_\theta\frac{\partial\Theta}{\partial z} - \nu_\Theta\left\langle\frac{\partial\Theta}{\partial z}\right\rangle, \tag{5}$$

where ν_θ and ν_Θ are called fluctuating and mean-filed eddy diffusivity for heat, respectively, ν_θ is still computed using the Smagorinsky model, but ν_Θ is calculated in a manner similar to ν_T .

At first, ν^*_Θ, the mean-filed eddy diffusivity for heat at the first grid level $z = z_1$ is calculated by

$$\nu^*_\Theta = \frac{kz_1}{\theta_* \phi_h(z_1)} \left(\langle w\theta \rangle - \langle w\theta \rangle_0 \right) - \langle \gamma \nu_\theta \rangle , \tag{6}$$

where, $\langle w\theta \rangle_0$ is the surface heat flux which is specified as the bottom condition in TASS model, and θ_* is the surface layer temperature scale. At the any other grid level $z > z_1$, ν_Θ is obtained by:

$$\nu_\Theta = \frac{\nu_T}{\nu^*_T} \nu^*_\Theta . \tag{7}$$

2.4. EMPIRICAL FORMS OF ϕ_m AND ϕ_h

The expressions of fluctuating eddy viscosity (ν_t) and eddy diffusivity of heat (ν_θ) contain the Monin–Obukhov similarity functions which need to be specified.

Under stable conditions, the most commonly used forms of ϕ_m and ϕ_h are:

$$\phi_m = 1 + 5\zeta, \tag{8}$$

$$\phi_h = \phi_h(0) + 5\zeta, \tag{9}$$

in which $\phi_h(0)$ has a value between 0.9 and 1.0.

But some investigators (Hicks, 1976; Holtslag and De Bruin, 1988) have found that the above expressions are not consistent with observations when ζ is greater than 1. Beljaars and Holtslag (1991) proposed the following empirical expressions for the related profile similarity functions:

$$-\Psi_m = a\zeta + b(\zeta - c/d) \, exp(-d\zeta) + bc/d, \tag{10}$$

$$-\Psi_h = \left(1 + \tfrac{2}{3} a\zeta\right)^{3/2} + b(\zeta - c/d) \, exp(-d\zeta) + bc/d - 1 \quad , \tag{11}$$

in which the suggested values of constants are: $a = 1, b = 0.667, c = 5, d = 0.35$. The value $a = 1$ is chosen so that the critical flux Richardson number $R_{fc} = 1$. Other constants are presumably based on the empirical estimates of these functions, which have large errors.

Recognizing the relations between Ψ_m and ϕ_m, and Ψ_h and ϕ_h,

$$\Psi_m = \int_0^\zeta \frac{1 - \phi_m(\zeta)}{\zeta} \, \mathrm{d}\zeta, \tag{12}$$

$$\Psi_h = \int_0^\zeta \frac{1 - \phi_h(\zeta)}{\zeta} \, \mathrm{d}\zeta, \tag{13}$$

one can obtain the corresponding expressions for ϕ_m and ϕ_h as:

$$\phi_m = 1 + \left[a + b\,(1 + c - \mathrm{d}\zeta)\,exp\,(-\mathrm{d}\zeta)\right]\zeta, \tag{14}$$

$$\phi_h = 1 + \left[a\left(1 + \tfrac{2}{3}a\zeta\right)^{1/2} + b\,(1 + c - \mathrm{d}\zeta)\,exp\,(-\mathrm{d}\zeta)\right]\zeta. \tag{15}$$

Equations (14) and (15) are utilized in the proposed SGS model to calculated ν_T^* and ν_Θ^*.

3. Simulation Parameters

A series of simulations of SBL with different stabilities are performed using TASS-LES. Most of the simulations have the same initial conditions but different geostro phic winds. Initially, the wind velocity is in geostrophic balance and a barotropic environment is assumed with the geostrophic wind in the x direction ($V_g = 0$). Periodic boundary conditions are applied in the horizontal directions. In vertical direction, a sponge layer with three grid intervals has been added on the top of physical domain. There exists neither heat nor mass transfer on the top boundary. The lower boundary employs a no-slip condition. The surface heat flux is specified as a function of time.

Our first simulation of the weakly stable boundary layer (WS0) is performed using the same large model domain (2000 m $\times$ 2000 m $\times$ 750 m) and coarse horizontal grid resolution ($\Delta x = \Delta y = 40$ m, $\Delta z = 10$ m) as used for simulating slightly unstable and neutral cases (Ding *et al.*, 2000). The initial potential temperature is specified 300 K below 450 m; it increases by 8 K across the 60 m inversion layer (from 450 m to 510 m) and further increases with a gradient of 3 K km^{-1} above 510 m. Initially, winds are in geostrophic balance, assuming a barotropic environment with a geostrophic wind speed in the x direction ($U_g =$ 15 m s^{-1}, $V_g = 0$). The results of the simulation of the previous neutral case (Ding *et al.*, 2000) serve as the initial field for this simulation, which is run for an additional 3 h. During those 3 h, the surface heat flux is gradually reduced from 0 to -0.04 K m s^{-1} during the first hour, and from -0.04 K m s^{-1} to -0.05 K m s^{-1} during the second hour. Then, the constant heat flux of -0.05 K m s^{-1} is maintained during the last hour.

Other simulations of stable cases are performed using smaller domains (500 m $\times$ 500 m $\times$ 500 m or 1000 m $\times$ 1000 m $\times$ 500 m) and finer horizontal grid resolutions ($\Delta x = \Delta y = 10$ m, or $\Delta x = \Delta y = 20$ m). The initial potential temperature is the same (300 K) below 320 m; it increases by 4 K across 30 m inversion layer (from 320 m to 350 m) and further increases with height with a smaller gradient of 3 K km^{-1} above 350 m. The number of grid points in x, y and z directions are 50 $\times$ 50 $\times$ 50. For different simulations, different combinations of grid size, domain size, and geostrophic wind speed (U_g) are given. All theses parameters are listed in Table I, in which WS0, WS1, and WS2 represent weakly stable cases, and MS1 and MS2 represent moderately stable cases.

Table I. The specified simulation parameters, the resulting scaling parameters and the bulk Richardson number for different cases

Cases	WS0	WS1	WS2	MS1	MS2
Δx, Δy, Δz (m)	40, 40, 10	10, 10, 10	10, 10, 10	10, 10, 10	20, 20, 10
L_x, L_y, L_z (m)	2000, 2000, 750	500, 500, 500	500, 500, 500	500, 500, 500	1000, 1000, 500
U_g (ms^{-1})	15	10	10	7.5	7.5
u_* (ms^{-1})	0.4241	0.3388	0.3114	0.1998	0.1924
L (m)	110.2	148.8	77.0	29.5	27.3
R_{iB}	0.140	0.136	0.144	0.256	0.270
h (m)	460	300	230	140	150

Total simulation time is 6.5 h. At first, the model is run for 1 h simulation time under the positive surface flux of 0.1 K m s^{-1} to generate a well-mixed turbulence field. Then, another 2 h simulation is performed after setting the surface heat flux to zero. Finally, the simulation is run for an additional 3.5 h when the surface heat flux is negative and specified as a function of time. During those 3.5 h, for cases WS1, MS1, MS2, the surface heat flux decreases from 0 to -0.015 K m s^{-1} during the first hour, and from -0.015 K m s^{-1} to -0.02 K m s^{-1} during the second hour. Then, the constant heat flux of -0.02 K m s^{-1} is maintained in the last 1.5 h. For case WS2, the surface heat flux is reduced to -0.02 K m s^{-1} at $t = 4$ h and -0.03 K m s^{-1} at $t = 5$ h. Figure 1 shows the specified variations of surface heat flux with time during the last 3.5 h. In this, the solid line represents the function for cases WS1, MS1 and MS2, the dashed line for the WS2 case, and the dotted line for WS0 case. These are typical of the real atmosphere during the first few hours after the sunset, although the minimum heat flux may vary from day to day. The last 60 min of the simulation is also used for obtaining averages and other analyses.

4. Simulation Results

In response to the decrease in the surface heat flux with time (Figure 1), Figure 2 shows the corresponding evolution of the domain-averaged TKE for the weakly stable case WS0 and moderately stable case MS1 during the last 3.5 h of simulation. Other cases have the similar shapes of TKE evolution curves with different initial values when heat flux is zero, due to different geostrophic winds. The domain-averaged TKE decreases rapidly during the first 60 min when the surface heat flux was changed to negative value. Then it decreases more gradually as the surface heat flux continues falling and reaches its minimum value when the surface heat flux becomes constant. In the last 60 min, domain-averaged TKE remains almost

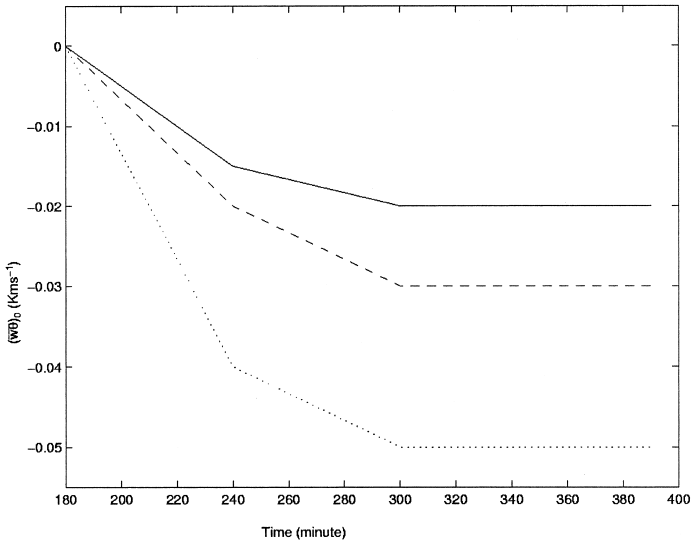

Figure 1. The specified surface heat flux as a function of time during the last 3.5 h of the simulation (solid line for case WS1, MS1 and MS2, dashed line for case WS2, and dotted line for WS0).

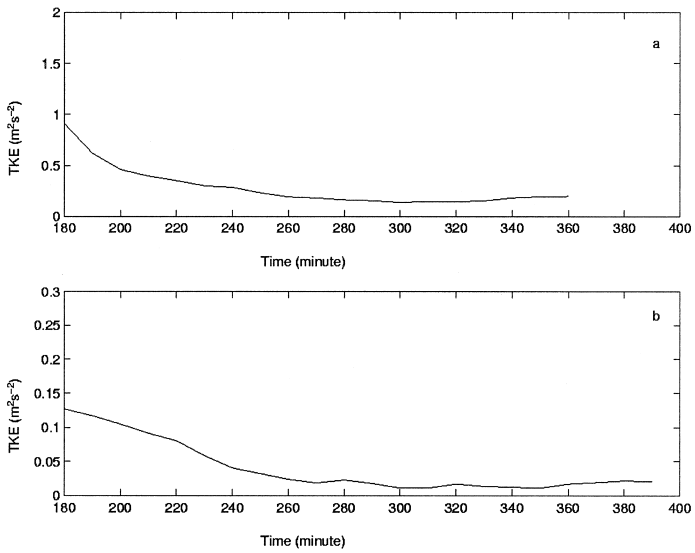

Figure 2. Time evolution of the domain-averaged TKE for (a) case WS0 and (b) case MS1 during the last 3.5 h of the simulation.

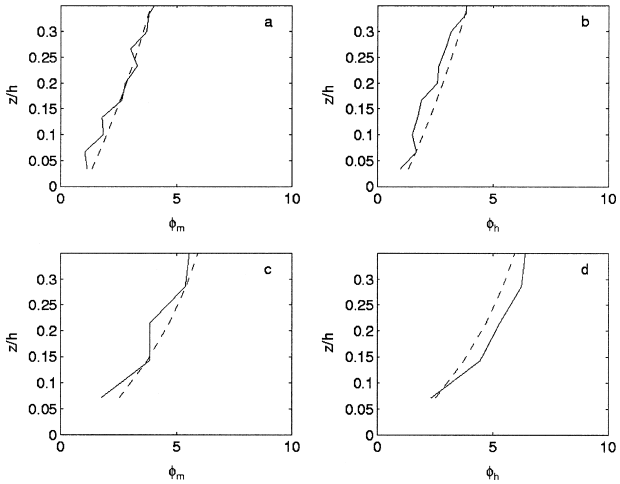

Figure 3. Comparison of simulated and empirical (measured) Monin–Obukhov similarity functions ϕ_m and ϕ_h in the lower part of SBL: (a) and (b) case WS1, (c) and (d) case MS1. Dashed line represents similarity theory, and solid line the simulation results.

constant. Thus, a quasi-steady state can be assumed to have been reached and the averaged results during the last 60 min can reveal the features of the SBL in quasi-steady state.

In Table I, we also list the ensemble averaged values of friction velocity (u_*), Monin–Obukhov length (L), the SBL height (h), and the bulk Richardson number (R_{iB}). It can be seen that the cases WS0, WS1, and WS2 have friction velocities greater than 0.3 m s^{-1}, bulk Richardson number less than 0.2, and Obukhov length greater than 70 m. Therefore, they are classified as weakly stable cases. The cases MS1 and MS2 have friction velocities less than 0.2 m s^{-1}, bulk Richardson number greater than 0.2, and Obukhov less than 30 m. These are characteristics of a moderately stable boundary layer rather than a strongly stable boundary layer. In this section, simulation results are discussed and differences between weakly and moderately stable cases are pointed out.

4.1. ENSEMBLE-AVERAGED PROFILES

Figure 3 shows the computed Monin–Obukhov similarity functions of ϕ_m and ϕ_h from the simulations (solid line) of case WS1 (Figures 3(a) and 3(b)) and MS1 (Figures 3(c) and 3(d)). These are compared with empirical similarity relations (14) and (15) for the surface layer (dashed line). It can be seen that model results from both cases closely agree with the surface layer similarity relations near the surface. And the agreement extends to about 0.25 h. The ϕ_m and ϕ_h profiles from case WS1 have slightly less deviation from the similarity theory than those from case MS1. All these reveal that under weakly to moderately stable conditions, the excessive

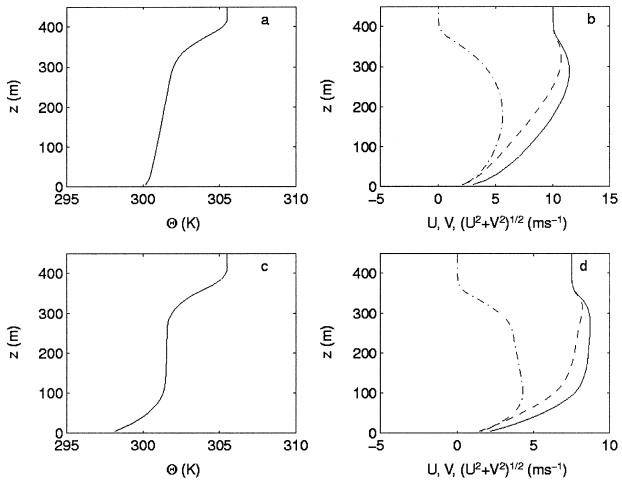

Figure 4. Ensemble-averaged profiles from the simulation of case WS1 and MS1: (a) and (b) case WS1, (c) and (d) case MS1. (a) and (c) potential temperature profile; (b) and (d) profiles of wind speed and its two components, solid line $M = (U^2 + V^2)^{1/2}$, dashed line U, dashed-dot line V.

wind shears near the surface resulting from the original Smagrinsky model are considerably reduced by using the proposed SGS model.

Figure 4 illustrates the ensemble-averaged profiles of wind speed, horizontal velocity components, and potential temperature from both the WS1 (Figures 4(a) and 4(b)) and MS1 cases (Figures 4(c) and 4(d)). Although these profiles have the typical observed shapes in the SBL, they also reveal differences between weakly SBL and moderately SBL. In case WS1, the potential temperature profiles clearly show a three-layer structure: a stable surface layer of strong gradients, a middle layer of small gradients, and an inversion layer on the top. These are similar to the results from Kosovic and Curry (2000), except that they defined a fourth layer as the layer above the top inversion layer. In case MS1, the potential temperature profile has a three-layer structure as well. However, the lower layer in this simulation has much stronger gradients, while the middle layer has almost zero gradient and is totally detached from the underlying SBL. The residual layer in WS1 simulation is shallower because of the deeper SBL in that case. The wind speed profiles in two cases all reveal the formation of the nocturnal low-level jet (LLJ). In case WS1, the maximum wind speed occurs at the height about 300 m. But in case MS1, it shows a rather broad maximum spanning the entire depth of the residual layer from about 140 m to 300 m. If we define the LLJ intensity as $(M_{\max} - U_g)/U_g$, then two cases have nearly the same LLJ intensities. The LLJ intensity for case WS1 is about 19%, and for case MS1 about 17%. The time evolution of the LLJ in response to decreasing surface heat flux is shown in Figure 5 for the WS0 case for which wind profiles are similar to those for other weakly stable cases.

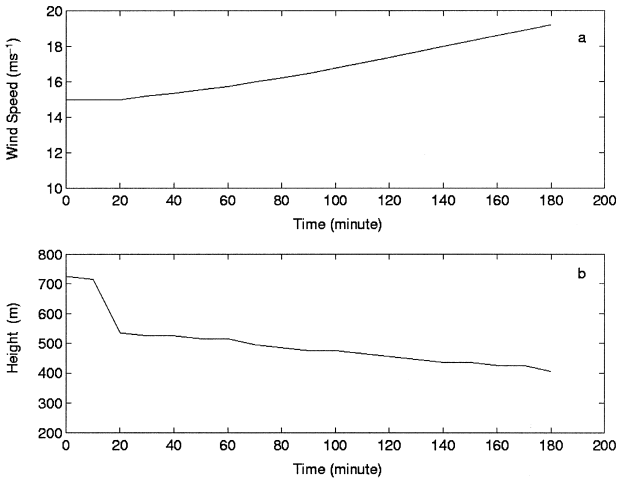

Figure 5. Evolution of LLJ for case WS0 during the last 3 h of the simulation: (a) maximum wind speed , and (b) corresponding height.

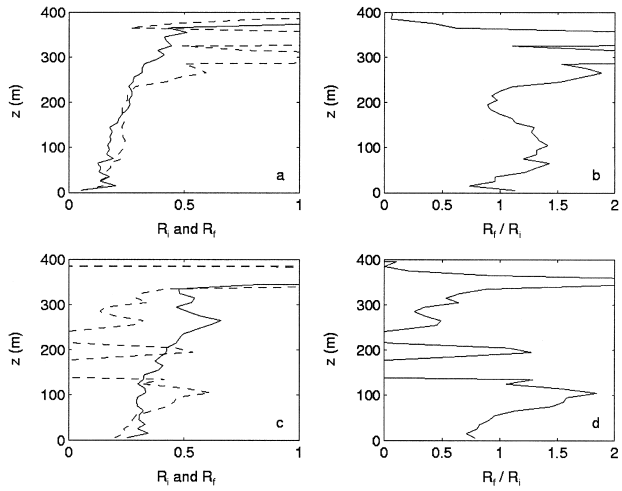

Figure 6. Profiles of gradient and flux Richardson number and their ratio from the simulation of case WS1 and MS1: (a) and (b) case WS1, (c) and (d) case MS1. (a) and (c) profiles of R_i and R_f, solid line R_i, dashed line R_f, (b) and (d) R_f/R_i.

Figure 6 shows the profiles of gradient Richardson number (solid line), flux Richardson number (dashed line) and their ratio for the two cases. In case WS1, the gradient Richardson number increases with height (more or less linearly) and attains its critical value near the top of the SBL whose height is about 300 m. Above 370 m it increased sharply to more than one. The profile of flux Richardson number has the similar shape except that above the SBL R_f alternately increases and de-

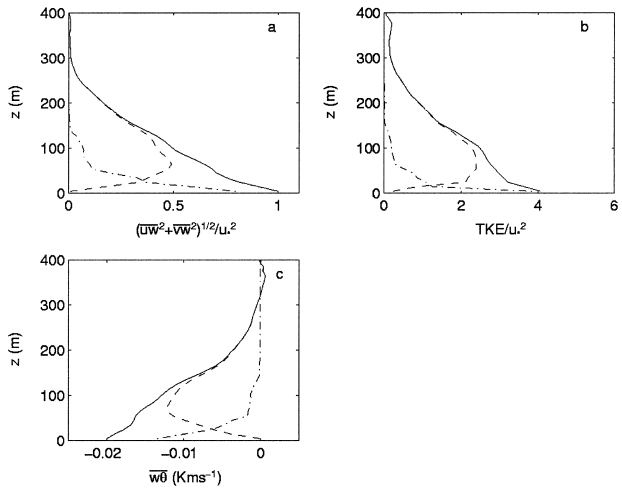

Figure 7. Vertical profiles of (a) horizontal momentum flux, (b) TKE/u_*^2, and (c) heat flux from the simulation of case WS1; solid line represents total, dashed line resolved part, dashed-dot line subgrid part.

creases sharply with height. These alternative increasing and decreasing must relate to the very small values of heat flux and momentum flux (shown later). The R_i and R_f profiles in this case are very similar to the results of NLHRB case from Kosovic and Curry (2000). Their NLHRB case is also a weakly stable boundary layer case. In case MS1, near the surface, R_i increases rapidly with height and attains its critical value. In the outer layer of this SBL, it keeps almost constant value slightly greater than critical value. In the residual layer, R_i further increases with the height almost linearly up to the base of the upper inversion layer. Within the inversion layer, like case WS1, gradient Richardson number increases sharply to more than one. The flux Richardson number increase with height up to about 100 m, and then decreases with height up to the top of this SBL. Within the residual layer and the upper inversion layer, it repeats the alternative increasing and decreasing like in case WS1. The profiles of the ratio of flux Richardson number to gradient Richardson number show that R_f/R_i has a value of around one in the most part of SBL. Because the ratio of R_f/R_i is equivalent to the ratio of eddy diffusivity for heat to that for momentum (K_H/K_M), our assumption of changing $K_H/K_M = 3$ for convective boundary layer to $K_H/K_M = 1$ for SBL is reasonable. Note that the diffusivity ratio or R_f/R_i apparently increases with height in the lower part of the SBL then decreases in the upper part.

Figures 7 and 8 give the vertical profiles of horizontal momentum flux, TKE, and heat flux from the simulations of WS1 (Figure 7) and MS1 (Figure 8). In both cases, the resolved parts dominate above 0.25 h, while near the surface the SGS contributions are larger. But in case MS1, the resolved parts comprise smaller percentage of total TKE and fluxes than those in case WS1. Both the momentum

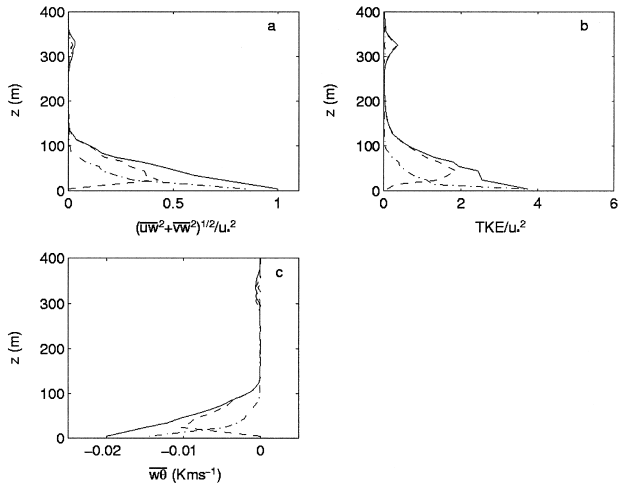

Figure 8. Same as Figure 7, but from case MS1.

and heat fluxes decrease almost linearly in the lower part of the SBL. The height of SBL can be defined as where momentum flux decreases to about 5% of its surface value. This definition is similar to that used by Kosovic and Curry (2000), who defined the SBL top as the level at which the tangential turbulent stress vanishes. The height level of vanishing turbulent stress or momentum flux may not be determined precisely. Note that the near surface value of TKE/u_*^2 in case MS1 is about 3.8 which is only slightly less than the value 4.1 in case WS1. However, they are much less than the typical value of 5.5 under the neutral condition.

4.2. TURBULENCE DECAY PROCESS

Figures 9 and 10 show the TKE and R_i profiles at 4 times during the turbulence decay process for case WS1 (Figure 9) and MS1 (Figure 10). The four times after the start of simulation are: 200 min (Figures 9(a) and 9(b), 10(a) and 10(b)), 250 min (Figures 9(c) and 9(d), 10(c) and 10(d)), 300 min (Figures 9(e) and 9(f), 10(e) and (f)), and 350 min (Figures 9(g) and (h), 10(g) and (h)). Both cases show that the TKE decays first in the region where R_i is large. For example, at $t = 300$ min in case WS1 (Figure 9(e)), the R_i values above 250 m are obviously larger than the values in the lower part. From the corresponding TKE profile in Figure 9(f), we find the TKE above 250 m decreased more rapidly than the TKE below 250 m. At $t \geq 250$ min in case MS1 (Figures 10(c), 10(e), and 10(g)) R_i attained large values above 150 m. The corresponding TKE profiles (Figures 10(d), 10(f), and 10(h)) show a rapid decrease of TKE in the 150–300 m layer. In case WS1, the R_i profile generally increases almost linearly with height. The larger R_i values occur in the upper part of SBL, and the decay of turbulence is a top-down process. The SBL depth decreased from about 400 m at $t = 200$ min to a near steady state value of

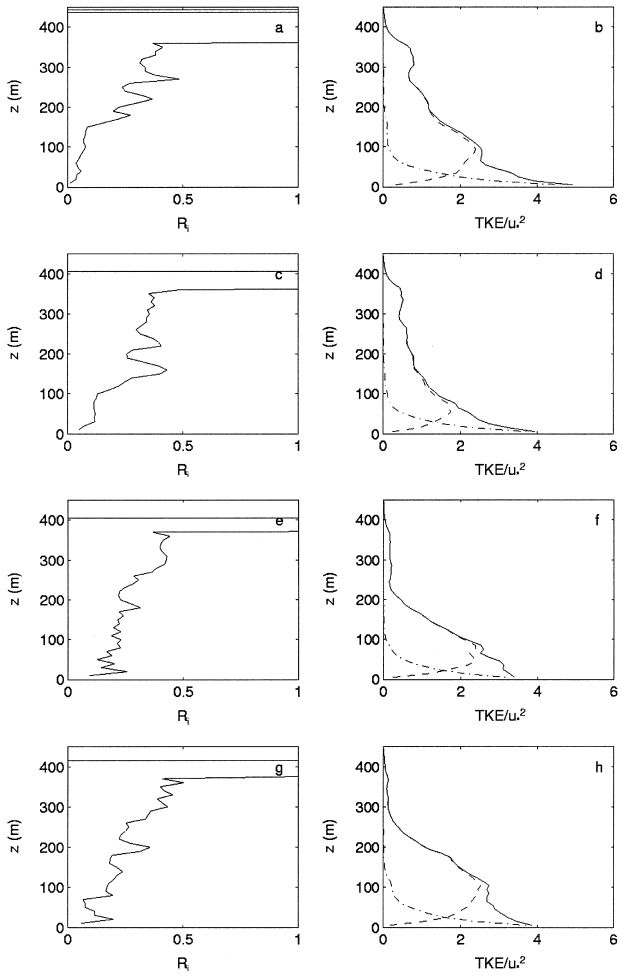

Figure 9. Vertical profiles of R_i and TKE/u_*^2 at 4 different times during the simulation of case WS1. (a) and (b) $t = 200$ min, (c) and (d) $t = 250$ min, (e) and (f) $t = 300$ min, (g) and (h) $t = 350$ min; solid line represents total, dashed line resolved part, dashed-dot line subgrid part.

about 300 m. For case MS1, the turbulence decay first occurs in the shallow layer of large R_i values between 200 m and 300 m and from there it extends up and down. Finally this region detaches from the underlying SBL and forms the residual layer.

Figures 11 and 12 give the TKE contours and R_i contours in a x–y cross section at the same 4 times ($t = 200$, 250, 300, 350 min) for both cases WS1 (Figure 11) and MS1 (Figure 12). The contours correspond to the height of about 0.5 h. From both cases, we find that the areas where larger R_i values occur (especially where

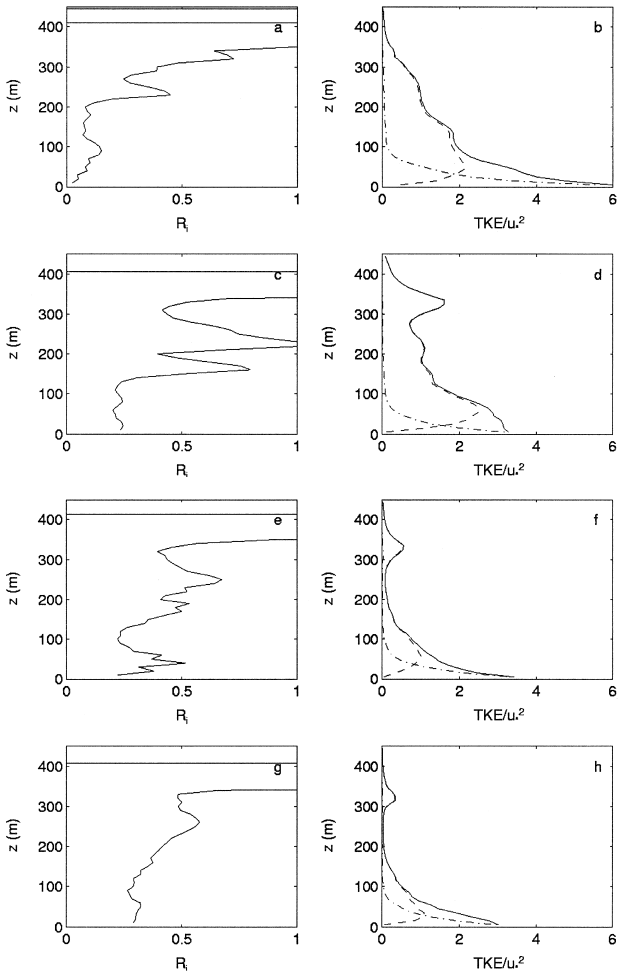

Figure 10. Same as Figure 9, but from case MS1.

$R_i > 0.25$) generally corresponds to the areas which have smaller TKE, but not *vice versa*, e.g., the lower-left part in Figures 11(c) and 11(d). In case WS1, the TKE contours show large areas of continuous turbulence in which R_i is less than R_{ic} (0.25). These are characteristic of the weakly stable boundary layer. In case MS1, at $t = 350$ min (Figures 12(g) and 12(h)), R_i values in nearly the entire domain are greater than R_{ic} (0.25), and the TKE contours reveal that turbulence becomes very sporadic and intermittent. These features are characteristic of a moderately stable boundary layer.

We have also investigated if there is a strong correlation between the instantaneous values of TKE and R_i for all the grid points used in the generation of contours

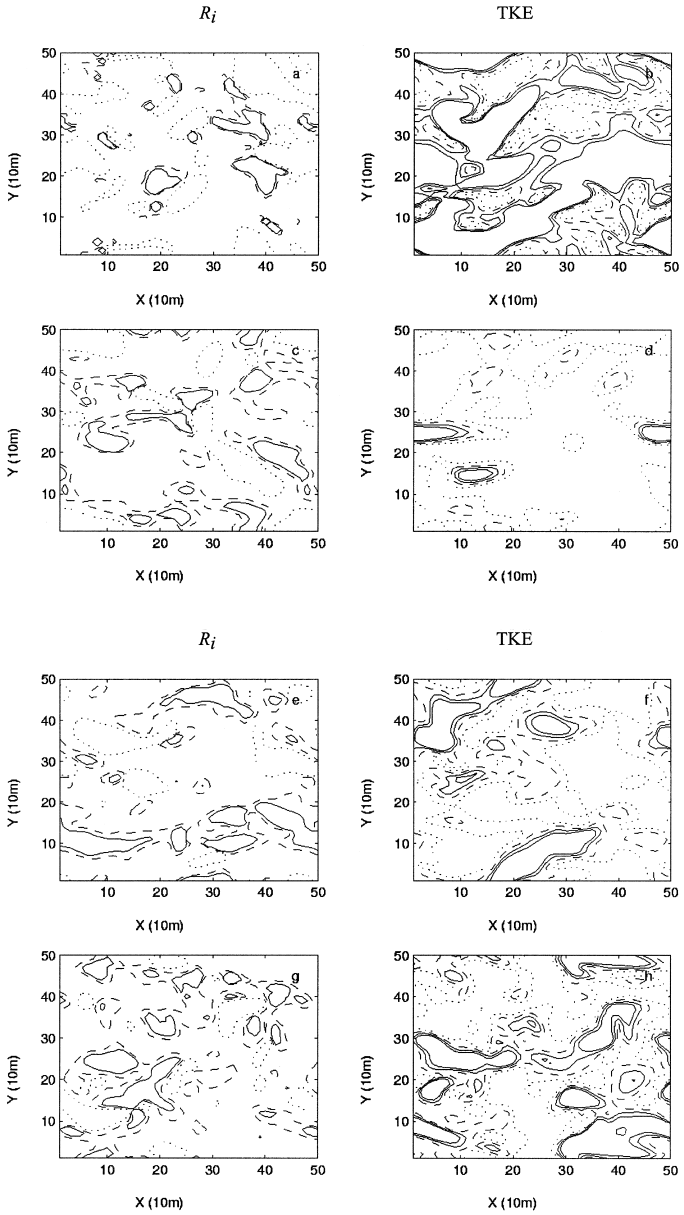

Figure 11. Contours of R_i and TKE at 4 different times during the simulation of case WS1. (a) and (b) $t = 200$ min, (c) and (d) $t = 250$ min, (e) and (f) $t = 300$ min, (g) and (h) $t = 350$ min. (a), (c), (e) and (g) R_i, dotted line 0, dashed line 0.25, solid line 0.5; (b), (d), (f) and (h) TKE, dotted line 0.05 m^2s^{-2}, dashed line 0.10 m^2s^{-2}, solid line 0.15 m^2s^{-2}or 0.20 m^2s^{-2}.

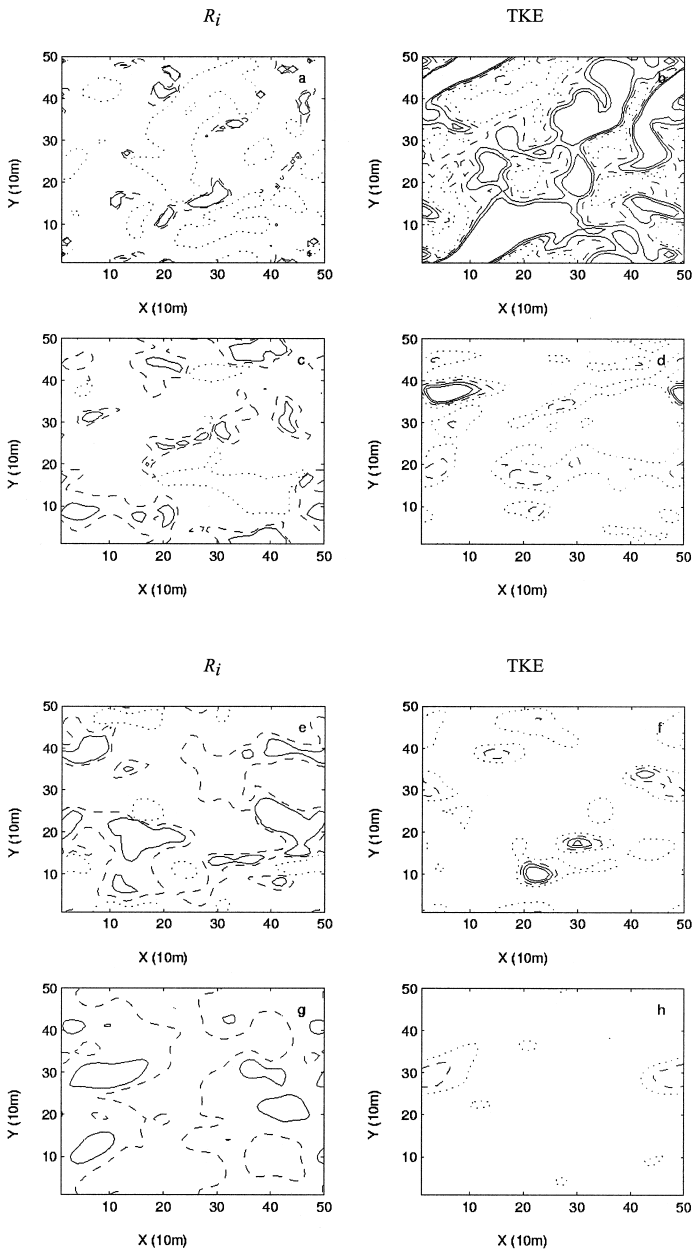

Figure 12. Same as Figure 11, but from case MS1.

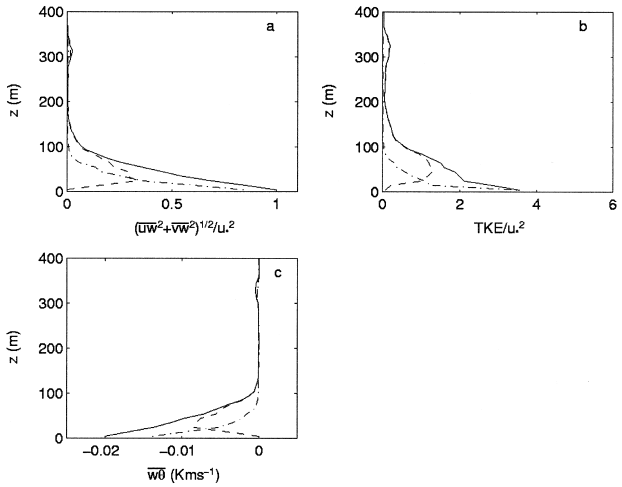

Figure 13. Vertical profiles of (a) horizontal momentum flux, (b) TKE/u_*^2, and (c) heat flux from the simulation of case MS2; solid line represents total, dashed line resolved part, dashed-dot line subgrid part.

in Figures 11 and 12 for the two cases. In both cases, we find that generally large R_i values are associated with small TKE values. But, there is considerable scatter of data (not shown), indicating that many grid points with small R_i can have small TKE and those with large R_i can have large TKE as well. Thus, there is not a unique relationship or very strong correlation between instantaneous values of R_i and TKE, as both the parameters appear to vary considerably in time and space.

4.3. SENSITIVITY TEST OF GRID SIZE OR RESOLUTION

In order the test the effect of grid size on LES, another simulation of moderately stable case MS2 is performed which has twice the horizontal grid size used in MS1 case. Figure 13 shows the vertical profiles of horizontal momentum flux, TKE and heat flux for this simulation. Compared with Figure 8, it can be seen that the two grid size cases gave very similar results, except that the resolved parts of the flux and TKE profiles of MS2 with the larger grid size comprise smaller percentage of the total fluxes and TKE than those in MS1. The comparison shows that with the proposed SGS model, a horizontal grid resolution of 10–20 m should be adequate for large-eddy simulation of the moderately stable boundary layer. A similar comparison of the simulated mean flow and turbulence structure in weakly stable cases WS0 and WS1 indicates that a larger horizontal grid size up to 40 m might be adequate for such cases.

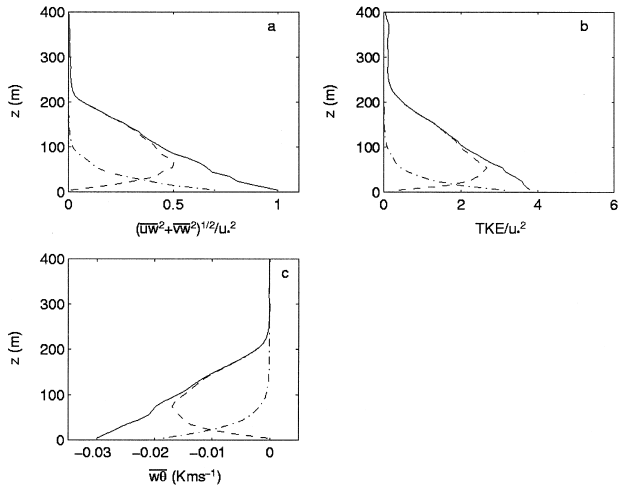

Figure 14. Same as Figure 13, but from case WS2.

4.4. SENSITIVITY TEST OF EXTERNAL FORCINGS

It is well known that more stable condition can be generated by either decreasing the surface heat flux or decreasing the geostrophic wind speed. To find the difference between two approaches, another simulation WS2 is performed which has the initial geostrophic wind speed of 10 m s^{-1}, but the surface heat flux is reduced more rapidly to -0.03 K m s^{-1} at $t \geq 300$ min (dashed line in Figure 1). Figure 14 gives the vertical profiles of horizontal momentum flux, TKE and heat flux for this simulation. The results from Figure 14 and Table I indicate that this simulation also represents a weakly stable boundary layer with $R_{iB} \approx 0.14$. Comparing the WS2 simulation with MS1, it can be seen that decreasing geostrophic wind speed is an easier way to generate more stable condition than decreasing surface heat flux. The WS0 case with the smallest heat flux turned out to be weakly stable because of the stronger geostrophic and simulated PBL winds.

5. Conclusions

A series of simulations of weakly to moderately stable boundary layers have been performed using the proposed SGS model implemented into TASS. The proposed SGS model incorporates some aspects of the two-part eddy viscosity SGS model of Sullivan *et al.* (1994). To simulate the SBL, further refinements are made; these include the dependence of SGS mixing length on stratification, two-part separation of the SGS eddy diffusivity of heat, and specifying more realistic empirical forms of Monin–Obukhov similarity functions.

The potential temperature profiles from both weakly and moderately SBLs clearly show a three-layer structure: a stable surface layer of strong gradients,

a middle layer of small gradients, and an inversion layer on the top. However, under moderate stability conditions, the lower layer has much stronger gradients, while the middle layer has almost zero gradient and is totally detached from the underlying SBL. The low-level jets (LLJs) are formed in all the cases. However, a rather broad maximum wind speed spans the entire depth of the residual layer in the simulation of moderately SBL. Both the momentum and heat fluxes decrease almost linearly in the lower part of the SBL. The near surface values of TKE/u_*^2 in all simulations are about 4 which is much less than the typical value of 5.5 under the neutral condition. The analyses of turbulence destruction and production in space and time illustrate that the decay of turbulence first occurs in the region with large Richardson number (R_i). Generally, the TKE decreases with increasing R_i, but there is no unique relationship between the instantaneous values of TKE and R_i at different grid points. A sensitivity test of grid size or resolution shows the simulation results are essentially independent of grid size and that horizontal gird resolution of 10–20 m should be sufficient for the large-eddy simulation of the moderately stable boundary layer. Another test of external forcings indicates that more stable boundary layers can be more easily simulated by decreasing the geostrophic wind, rather than by decreasing the surface heat flux alone.

Acknowledgements

We want to express our thanks to North Carolina Supercomputer Center for using its CRAY facility. The partial support of the Cooperative Agreement No. NCC-1-188 with NASA-Langley is also gratefully acknowledged.

References

A. Andren, The structure of stably stratified atmospheric boundary layers: A large-eddy simulation study . *Quart. J. Roy. Meteorol. Soc.* **121** (1995) 961–985.

A.C.M. Beljaars and A.A.M. Holtslag, Flux parameterization over land surfaces for atmospheric models. *J. Appl. Meteorol.* **30** (1991) 327–341.

R.A. Brost and J.C. Waynaard, A model study of the stably stratified planetary boundary layer. *J. Atmos. Sci.* **35** (1978) 1427–1440.

A. Brown, S.H. Derbyshire and P.J. Mason, Large-eddy simulation of stable atmospheric boundary layers with a revised stochastic subgrid model. *Quart. J. Roy. Meteorol. Soc.* **120** (1994) 1485–1512.

J.W. Deardorff, A three-dimensional numerical investigation of idealized planetary boundary layer. *Geophys. Fluid Dyn.* **1** (1970) 377–410.

J.W. Deardorff, Stratocumulus-Capped mixed layers derived from a three-dimensional model, *Bound.-Layer Meteorol.* **18** (1980) 495–527.

F. Ding, S.P. Arya and Y.-L. Lin, Large-eddy simulations of the atmospheric boundary layer using a new subgrid-scale model: Part I. Slightly unstable and neutral cases. *Environ. Fluid Mech.* **1** (2001) 29–47 (this issue).

B.B. Hicks, Wind profile relationships from the 'Wangara' experiments. *Quart. J. Roy. Met. Soc.* **102** (1976) 535–551.

A.A.M. Holtslag and H.A.R. De Bruin, Applied modeling of the nighttime surface energy balance over land. *J. Appl. Meteorol.* **27** (1988) 689–704.

H.J. Kaltenbach, T. Gerz and U. Schumann, Large-eddy simulation of homogeneous turbulence and diffusion in stably stratified shear flow. *J. Fluid Mech.* **280** (1994) 1–40.

B. Kosovic, Subgrid-scale modeling for the large-eddy simulation of high-Reynolds-number boundary layers. *J. Fluid Mech.* **336** (1997) 151–182.

B. Kosovic and J.A. Curry, A large-eddy simulation study of a quasi-steady, stably stratified atmospheric boundary layer. *J. Atmospheric. Sci.* **57** (2000) 1052–1068.

P.J. Mason, Large-eddy simulation of the convective atmospheric boundary layer. *J. Atmospheric Sci.* **46** (1989) 1492–1516.

P.J. Mason and D.J. Thomson, Stochastic backscatter in large-eddy simulations of boundary layers. *J. Fluid Mech.* **242** (1992) 51–78.

P.J. Mason and S.H. Derbyshire, Large-eddy simulation of the stably stratified atmospheric boundary layer. *Bound.-Layer Meteorol.* **53** (1990) 117–162.

C.-H. Moeng, A large-eddy simulation model for the study of planetary boundary layer. *J. Atmospheric. Sci.* **41** (1984) 2052–2062.

F.T.M. Nieuwstadt, The turbulent structure of the stable nocturnal boundary layer. *J. Atmos. Sci.* **41** (1984) 2202–2216.

F.H. Proctor, The Terminal Area Simulation System, Volume I: Theoretical formulation. NASA Contractor Report 4046 DOT/FAA/PM-86/50, I (1987).

F.H. Proctor, Numerical simulation of an isolated microburst. Part I: Dynamics and Structure. *J. Atmos. Sci.* **45** (1988) 3137–3159.

E.M. Saiki, C.-H. Meng, P.P. Sulivan, Large-eddy simulation of the stably stratified planetary boundary layer. Preprints, *13th Symposium on Boundary Layers and Turbulence*, Dallas, TX, January 10–15, 1999, American Meteorological Society, Boston, MA (1999) 211–214.

D.G. Schowalter, D.S. DeCroix, Y.-L. Lin, S.P.S. Arya and M.L. Kaplan, Planetary boundary layer simulation using TASS. NASA Contractor Report 198325, NASA Langley Research Center, Hampton, VA (1996a) 34 pp.

D.G. Schowalter, D.S. DeCroix, Y.-L. Lin, S.P.S. Arya and M.L. Kaplan, The sensitivity of large-eddy simulation of local and non-local drag coefficients at the lower boundary. NASA Contractor Report 198310, NASA Langley Research Center, Hampton, VA (1996b) 36 pp.

P.P. Sullivan, J.C. McWilliams and C.-H. Moeng, A subgrid-scale model for large-eddy simulation of planetary boundary layer. *Bound.-Layer Meteorol.* **71** (1994) 247–276.